Nuclear Instruments and Methods in Physics Research A 383 (1996) 301–308

ELSEVIER

NUCLEAR INSTRUMENTS & METHODS IN PHYSICS RESEARCH Section A

Different kinds of analysis methods on a rectangular combined function bending magnet

C.S. Hwang[a,b,*], C.H. Chang[a], P.K. Tseng[a,c,e], T.M. Uen[b], Joel Le Duff[d]

[a] *Synchrotron Radiation Research Center (SRRC), Hsinchu 30077, Taiwan*
[b] *Department of Electrophysics, National Chiao Tung University, Hsinchu, Taiwan*
[c] *Department of Physics, National Taiwan University, Taipei, Taiwan*
[d] *Laboratoire de l'Accelerateur Lineaire (LAL), Centre d'Orsay, France*
[e] *Department of Physics, Tamkang University, Tamsui, Taiwan*

Received 15 April 1996; revised form received 4 July 1996

Abstract

Magnetic field features of a rectangular combined function bending magnet are different from the sector magnet. A strong edge focusing factor (i.e., thin lens effect) intrinsically exists at the two magnet edges for the rectangular bending magnet. Therefore, in this study, we develop two kinds of Hall probe mapping trajectory with four analysis methods to measure and analyze the bending magnet's field behavior. A sufficient correlation among the four methods is an important feature. Those methods are individually used to derive the pole face tilt and bent, the effective magnetic length and to check the specification establish by the beam dynamics group. As for the two mapping methods, one is called "Radial Mapping" whose mapping trajectories in the longitudinal direction (s-axis) follow the different arc lengths of radius $\rho \pm r$ and the transverse trajectories follow the radial displacement $\pm r$ perpendicular to the arc trajectory. The other one is called "Lamination Mapping" whose mapping trajectories in the longitudinal direction follow the constant arc length of circle radius ρ and the transverse trajectories follow the transverse axis displacement $\pm x$ parallel to the lamination direction.

This study also discusses the differences between those two mapping methods. Results obtained from the harmonic field distribution along the longitudinal direction (including the fringing field) and the main components of the integral strength are compared. The subsequent error of the four analysis methods is 0.01% for the dipole strength and 0.3% for the quadrupole strength individually. According to the specifications, those analysis errors are acceptable. Meanwhile, the accuracies of different methods for the higher multipole strengths are all within tolerances. The peculiar sextupole field behavior at the two magnet edges from the different mapping methods is owing to the effective magnet pole face that will be discussed.

1. Introduction

The combined function bending magnet with rectangular hard-edges is normally operated at 1.3 GeV. The dipole magnet [1,2] with curvature radius $\rho = 3.495$ m, bending angle $2\Theta = 20°$ and magnetic length 1.22 m, produces an integral magnetic field of 1.5137 T m and a 1.957 T integral gradient strength. The Hall probe mapping system [3–5] was used to measure the magnetic field distribution. Simultaneously, the mapping methods and alignment procedure were developed to perform this task [6].

Mapping along the same coordinates is an appropriate measure since beam dynamics uses the curvilinear coordinate x–y–s system in the bending magnet. For a sector bending magnet with a tilt angle of $\alpha = 0°$ [7], the mapping trajectories in the longitudinal direction follow the different arc lengths of radius $\rho \pm r$; in addition, the transverse trajectories follow the radial displacement $\pm r$ perpendicular to the arc trajectory. This mapping method is defined as "Radial Mapping". However the SRRC bending magnet is a rectangular one with parallel lamination and a gradient along the direction of the laminations. The usual edge focusing effect of angle bending Θ can be modified if the effective pole faces are tilted and bent due to magnet saturation in the corners, finite pole width, unsymmetric magnet circuit (c-type magnet) and coils bent at the magnet edge. For those reasons, mapping the magnet along the lamination direction is an interesting task. This is also as double check of the accuracy of the magnet assembly. This mapping method is called "Lamination Mapping". The "Lamination Mapping" refers to a situation in which the transverse mapping trajectories follow

* Corresponding author.

PII S0168-9002(96)00801-7

the transverse axis displacement $\pm x$ and the longitudinal direction follow the constant arc of bending radius ρ. Properly treating the measurement data allows a cross check with the first method that is useful to estimate the analysis accuracy.

The analysis methods [8], according to these two mapping trajectories, are (A) From the "Radial Mapping" the magnetic field is expanded with respect to the radial coordinate r and then the field is integrated along the s-axis for each harmonic. (B) From the "Radial Mapping" the field is integrated first along s-axis and then expanded with respect to r. (C) From the "Lamination Mapping", the magnetic field is expanded with respect to the horizontal coordinate x and then the field is integrated for each harmonic. (D) From the "Lamination Mapping", the magnetic field is first integrated and then expanded with respect to horizontal transverse coordinate x.

The differences in the field integral strength among the four analysis methods have been found to be within 0.3% for the quadrupole integral strength and within 0.01% for the dipole integral strength. The higher multipole strengths beyond the sextupole field from the two mapping methods are also very close. The different behaviors of each harmonic at the magnet edge from the two mapping methods are also discussed. The sufficient correlation between the different analysis approaches demonstrates the effectiveness of the two mapping methods.

2. The mapping trajectory

Although the rectangular combined function magnet differs from a sector one, a curvilinear coordinate system x–y–s can be used. Since the measuring probe's position stage follows a rectangular coordinate system x–y–z, the relationship between these two systems must be defined. For the two mapping methods, the "Radial Mapping" (see Fig. 1a) and the "Lamination Mapping" (see Fig. 1b), the longitudinal s-axis trajectory is performed along a series of arcs inside the magnet of bending angle $|\Theta| \leq 10°$ and along straight lines outside the magnet ($\Theta > 10°$ and $\Theta < -10°$). The magnet center (0,0,0) is on the nominal trajectory ($j = 0$) of the TBA dipole magnet. The trajectories for each mapping method are described in the following:

2.1. Radial mapping method

Fig. 1a shows the "Radial mapping" trajectories. For the central magnet region ($|\Theta| \leq 10°$), the Hall probe either follows a displacement $\pm r$ in the radial direction perpendicular to the arc of radius $\rho \pm r$ or follows the arc trajectory with radius $\rho \pm r$. The outside magnet regions ($\Theta > 10°$ and $\Theta < -10°$) denote that Θ is constant at the upstream $\Theta = 10°$ and downstream $\Theta = -10°$. The Hall probe either follows a radial displacement $\pm r$ corresponding to a constant curvature radius ρ and perpendicular to the straight line trajectories (s-axis) or follows the parallel straight lines' trajectories which are tangential to the arc at the locations $\Theta = \pm 10°$.

2.1.1. Inner magnet region ($|\Theta| \leq 10°$)

Mapping along the radial direction

If Θ_i is the angle corresponding to the ith position on the s-axis (nominal trajectory $j = 0$), the coordinates of the jth position (in the radial direction) at the same ith position are with:

$$x_i = x_{i0} + \sum_j \Delta x_{ij}, \tag{1}$$

$$z_i = z_{i0} + \sum_j \Delta z_{ij}, \tag{2}$$

with:

$$\Delta x_{ij} = r \cos\Theta_i, \tag{3}$$

$$\Delta z_{ij} = r \sin\Theta_i, \tag{4}$$

where r is the elementary step between two consecutive mapping points in the radial direction. The mapping points on the nominal trajectory correspond to $j = 0$, where x_{i0} and z_{i0} are the initial positions of this radial direction mapping trajectory.

Mapping along the arcs

If S_{i0} is the elementary arc length between two consecutive mapping points on the nominal trajectory, and can be adjusted to a optimum length which is termed as the trapezoidal rule to get a high accuracy. The θ_i is the corresponding step angle which converts from length S_{i0} can be expressed as:

$$S_{ij} = S_{i0}[1 \pm j(r/\rho)], \tag{5}$$

$$\theta_i = S_{i0}/\rho, \tag{6}$$

with $\rho = 3.495$ m for the SRRC magnet. Mapping from 10° to −10° are gotten as:

$$\Theta = 10° - \sum \theta_i. \tag{7}$$

Coordinates of the ith mapping position (in the s-axis) at the same jth position are

$$x_j = x_{j0} + \sum_i \Delta x_{ji}, \tag{8}$$

$$z_j = z_{j0} + \sum_i \Delta z_{ji}, \tag{9}$$

with:

$$\Delta x_{ji} = (\rho \pm jr)(\cos\Theta - \cos 10°), \tag{10}$$

$$\Delta z_{ji} = (\rho \pm jr)(\sin\Theta - \sin 10°). \tag{11}$$

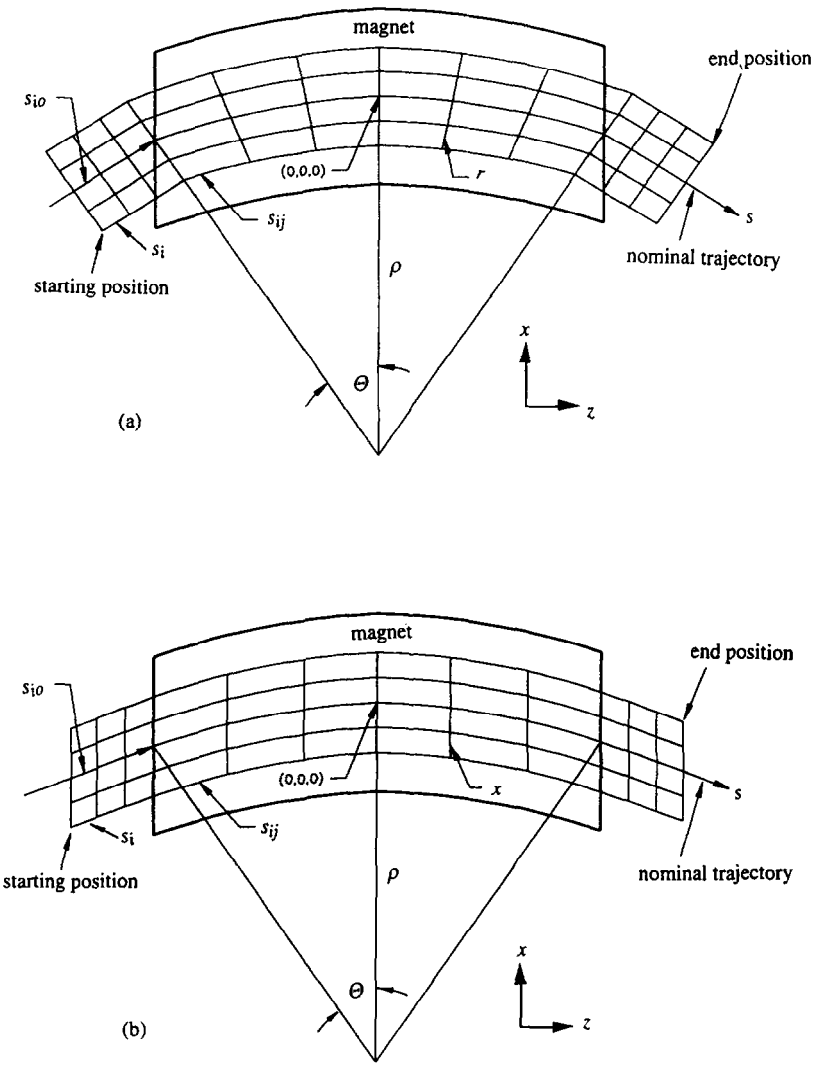

Fig. 1. (a) The mapping trajectories on the radial mapping method of TBA dipole magnet. (b) The mapping trajectories on the lamination mapping method of TBA dipole magnet.

where x_{jo} and z_{jo} are related to the initial position on the arc mapping trajectory.

2.1.2. Outside magnet region on the x–s plane

In this region, Θ is maintained constant (in the upstream $\Theta = 10°$ and downstream $\Theta = -10°$). The Hall probe either follows the straight line trajectories which are tangential to the arc at the location of $\Theta = \pm 10°$ or a radial displacement $\pm r$ corresponding to a constant curvature radius ρ and perpendicular to the straight line trajectory s-axis.

Mapping along the radial direction

In the radial direction mapping, Θ is maintained constant 10° or −10°. Hence, the coordinates of the jth mapping position (in the radial direction) at the same ith position are similar to Eq. (1) and Eq. (2) with

$$\Delta x_{ij} = r \sin 10°, \tag{12}$$

$$\Delta z_{ij} = r \cos 10°. \tag{13}$$

Mapping along the slope straight line trajectory

In the straight line mapping trajectory, the curvature radius ρ is maintained constant and $\Theta = \pm 10°$. S_i is the elementary straight length between two consecutive mapping points on the nominal trajectory, the straight length S_i depend on the variation of field strength distribution to set the value. Consequently, the coordinates of the ith mapping position on the jth straight line are similar to those as in Eq. (8) and Eq. (9) with

$$\Delta x_{ij} = S_i \sin 10°, \tag{14}$$

$$\Delta z_{ji} = S_i \cos 10°. \tag{15}$$

2.2. Lamination mapping method

Fig. 1b shows the corresponding mapping trajectories. For the central magnet region, the Hall probe either follows a displacement $\pm x$ in the lamination direction parallel to the coordinate x-axis or follows the arc trajectory s-axis with a constant curvature radial ρ. In the outside magnet region, the Hall probe either follows the same lamination displacement $\pm x$ corresponding to a constant curvature ρ or follows the parallel straight lines' trajectories which are tangential to the arc at the locations $\Theta = \pm 10°$.

2.2.1. Inner magnet region

Mapping along the lamination direction

Since the lamination direction is parallel to the x-axis, the lamination direction trajectory is independent of the angle Θ and the curvature radius ρ always remains constant. Therefore, the coordinates of the jth mapping position in the lamination direction are similar to those as in Eq. (1) and Eq. (2) with $\Delta x_{ij} = r$ and $\Delta z_{ij} = 0$.

Mapping along the arcs

That parallel arcs lengths are the same with a constant curvature radius ρ inside the magnet region. Therefore, the coordinates of the ith mapping position at the same jth position are similar to those in Eq. (8) and Eq. (9) with

$$\Delta x_{ji} = \rho(\cos\Theta - \cos 10°), \tag{16}$$

$$\Delta z_{ji} = \rho(\sin\Theta - \sin 10°). \tag{17}$$

2.2.2. Outside the magnet region

Mapping along the lamination direction

In this mapping trajectory, the trajectory is also parallel to x-axis. Therefore, the coordinates of the jth mapping point in the lamination direction are similar to those in Eq. (1) and Eq. (2) with $\Delta x_{ij} = r$ and $\Delta z_{ij} = 0$.

Mapping along the straight line

Those parallel straight line trajectories are tangential to the arc at $\Theta = \pm 10°$. Where S_i is the elementary straight length between two consecutive mapping points on the nominal trajectory, the straight length S_i depends on the variation of field strength distribution to set the value. Then the coordinates of the ith mapping position at the same jth position are similar to those in Eq. (8) and Eq. (9) with Eq. (14) and Eq. (15).

3. Analytical methods

3.1. From the radial direction mapping

Examining the particles trajectories in a static field normally requires representing the field in a curvilinear coordinate system that refers to the nominal trajectory. This system is referred to as the radial system. In a magnet having a horizontal symmetry plane (midplane), only the vertical field component $B_y(r,s)$ in this plane must be known. The nonlinear content of the field can be directly obtained from the "radial mapping" by expanding the field in radial direction r

$$B_y(r,s) = B_{er}(s) + G_{er}(s)r + S_{er}(s)r^2 + O_{er}(s)r^3 + D_{er}(s)r^4 + \cdots \tag{18}$$

and then performing the integral of each component along the nominal path so that

$$\int B_y(r,s)\,\mathrm{d}s = \int B_{er}(s)\,\mathrm{d}s + \left[\int G_{er}(s)\mathrm{d}s\right] r + \left[\int S_{er}(s)\,\mathrm{d}s\right] r^2 + \left[\int O_{er}(s)\,\mathrm{d}s\right] r^3 + \cdots. \tag{19}$$

The gradient integral $\int G_{er}(s)\,\mathrm{d}s$ includes the thin lens focusing effect $\{-(B\rho)\tan\Theta/\rho\}$ due to the pole face tilts, with respect to a pure sector magnet, at both ends of the magnet. This is because beam dynamics codes already used thin lens approximation. Hence, the gradient field $\int G\,\mathrm{d}s$ of the beam dynamics codes is then given by

$$\int G\,\mathrm{d}s = \int G_{er}(s)\,\mathrm{d}s - [-2\tan\Theta/\rho][B\rho]. \tag{20}$$

and the fundamental and other multipole strength in Eq. (19) does not need to be modified and is equal to the beam dynamics use.

Another method to analyze the nonlinear content of the field consists of determining the magnet effective length as a function of r. In that case, the $B_y(r,s)$ field is measured and integrated along different parallel arcs on the longitudinal direction will give us the different magnetic length which would be similar to the effective length of sector magnet. Hence, the vertical field $B_y(r,s)$ on the midplane can be integrated and corresponding straight lines on both sides of the magnet as:

$$\int B_y(r,s)\,\mathrm{d}l = \int B_y(r,s)[(\rho + r)\,\mathrm{d}\theta] = \int B_y(r,s)\,\mathrm{d}s + \left(\int B_y(r,s)\,\mathrm{d}s/\rho\right) r = \int B\,\mathrm{d}s + \int [G + (B/\rho)]\,\mathrm{d}s\, r + \int [S + (G/\rho)]\,\mathrm{d}s\, r^2 + \cdots. \tag{21}$$

where $dl = (\rho \pm r)d\theta$. The field integral is then expanded into

$$\int B_y(r,s)dl = \int B_{ir}ds + \int G_{ir}ds\, r + \int S_{ir}ds\, r^2 + \int O_{ir}ds\, r^3 + \int D_{ir}ds\, r^4 + \cdots. \quad (22)$$

Identification between Eq. (21) and Eq. (22) leads to

$$\int Bds = \int B_{ir}ds,$$

$$\int Gds = \int [G_{ir} - B_{ir}/\rho]ds - [-2\tan\Theta/\rho][B/\rho],$$

$$\int Sds = \int S_{ir}ds - [\int G_{ir}ds]/\rho + [\int B_{ir}ds]/\rho^2. \quad (23)$$

Again, the gradient integral $\int G_{ir}\, ds$ includes the edge thin lens effects. Hence, the gradient field $\int G\, ds$ to be used in the beam dynamics is obtained by twice subtracting the previous quantity to the total gradient field strength.

3.2. From the lamination direction mapping

Since the magnet assembly is made of parallel laminations displayed along the nominal path, so having parallel pole face (rectangular magnet), it is also of interest to expand the $B_y(x,s)$ field along the direction x-axis of the lamination to check the field quality. This is obtained directly from the "lamination mapping" by expanding the field in the lamination direction x:

$$B_y(x,s) = B_{el}(s) + G_{el}(s)x + S_{el}(s)x^2 + O_{el}(s)x^3 + D_{el}(s)x^4 + \cdots \quad (24)$$

and then performing the integral of each component along the nominal path so that

$$\int B_y(x,s)\, ds = \int B_{el}\, ds + \int [G_{el}(s)\, ds]x + \int [S_{el}(s)\, ds]x^2 + \int [O_{el}(s)\, ds]x^3 + \cdots, \quad (25)$$

where $G_{el}(s)$ here represents the physical gradient related to the shaping of the lamination. Since a mapping point (θ,r) has for its coordinate in the lamination system:

$$x = r/\cos\theta. \quad (26)$$

Eq. (26) was put into Eq. (25) and by the multipole expansion definition one will obtain the Eq. (27)

$$\int B_y(x,s)\, ds = \int B(s)\, ds + \int G(s)\cos\theta\, ds\, x + \int S(s)\cos^2\theta\, ds\, x^2 + \int O(s)\cos^3\theta\, ds\, x^3 + \cdots. \quad (27)$$

By considering the magnet gradient $\int G(s)\, ds$ which is of interest in beam dynamics studies, it can be deduced from the lamination gradient which by construction should remain approximately constant within the magnetic length:

$$\int G(s)\, ds = \rho G_{el}(0)\int_{-\Theta}^{\Theta} \frac{d\theta}{\cos\theta} \quad (28)$$

where $G_{el}(0)$ is considered to remain constant within the effective length of the magnet:

$$L_{G_{\text{eff}}} = \int G_{el}(s)\, ds/G_{el}(0). \quad (29)$$

With radius $\rho = 3.495$ m, the magnet effective length $L_{G_{\text{eff}}} = 1.222$ m and the bending angle $\Theta = 10°$, one obtains

$$\int G\, ds = 2\frac{\rho\int G(s)_{el}\, ds}{L_{G_{\text{eff}}}}(\ln|\sec\Theta + \tan\Theta|) = 1.003\int G(s)_{el}\, ds. \quad (30)$$

In checking the magnet properties, the field integral can be measured at different values of x to obtain the magnet length as a function of x for comparison with the ideal hard-edge magnet. Expanding the field integral of the lamination direction mapping with respect to x will give the nonlinear components as

$$\int B_y(x,s)\, ds = \int B_{il}(s)\, ds + \int [G_{il}(s)\, ds]x + \int [S_{il}(s)\, ds]x^2 + \int [O_{il}(s)\, ds]x^3 + \cdots. \quad (31)$$

Eq. (31) must be equal to Eq. (25). Therefore, the final result of $\int G\, ds$ is also equal to be $1.003\int G_{il}(s)\, ds$. The corresponding nonlinear components, however, require a special treatment before they can be used in beam dynamics calculations.

4. Measurement and analysis results

The magnet was measured by the home made Hall probe measurement system [3–5]. The harmonic content along the s-axis between the two mapping methods has a quite different behavior except the dipole field strength. Fig. 2 shows that the dipole field distribution on the longitudinal axis is almost the same between the two mapping methods. However, for a higher multipoles strength, the difference is quite important for the beam dynamics behavior. Fig. 3 shows the quadrupole field distribution along the s-axis and Table 1 shows the integral field strength of each harmonic according to Eq. (19), Eq. (22), Eq. (25) and Eq. (31). Fig. 2 reveals that the dipole field strength at the magnet edge becomes negative and then goes to zero far

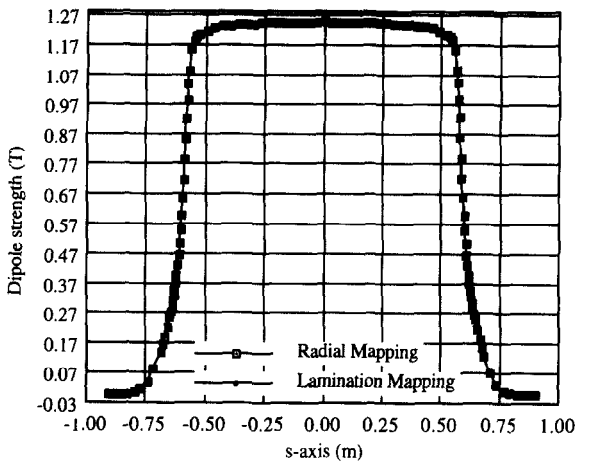

Fig. 2. Dipole field distribution along the longitudinal direction of the two mapping methods.

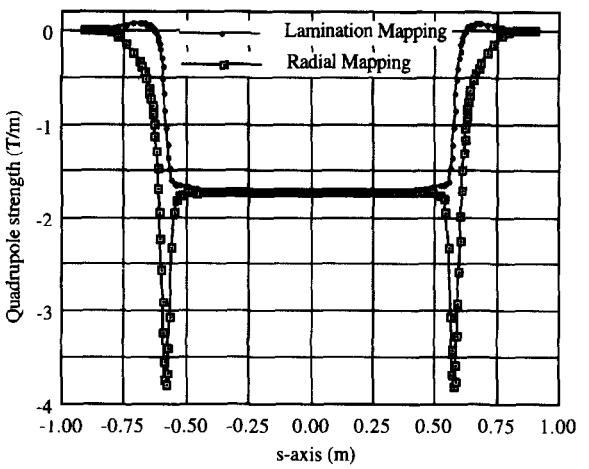

Fig. 3. Quadrupole field distribution along the longitudinal direction of the two mapping methods.

away from the magnet. The negative field strength is due to the fringe field of the coil. Fig. 3 shows a strong negative quadrupole field at the two edges with the "Radial Mapping" method, corresponding to the thin lens effect from the pole face rotation. With the "Lamination Mapping" method, the negative quadrupole field is smooth; it then becomes positive and finally goes to zero far away from magnet. This positive quadrupole field behavior also originates from the fringing of the coil similar to the dipole field behavior.

The integrated gradient and higher multipole strengths must be unified to obtain the useful value for beam dynamics use. Therefore, the integrated gradient strength $\int G\,ds$ of the Eq. (19), Eq. (22), Eq. (25) and Eq. (31) has been calculated according to Eq. (20), Eq. (23) and Eq. (30). The unify integrated harmonic strength is the field strength modification only within the effective magnetic length region ($|\Theta| \leq 10°$) and plus the non-modification field strength outside the effective magnetic length region ($\Theta > 10°$ and $\Theta < -10°$). Therefore, Table 2 presents the final value $\int G\,ds$ and the higher multipole integral strength will be used in beam dynamics.

The maximum error on these integral $\int G\,ds$ between the different methods is about 0.006 T. This error normalized to the nominal quadrupole integrated strength is about 0.3%. The largest error derives from the lamination mapping methods. The error is primarily owing to the assumption made in the analysis process (Eq. (28)). This is because the "radial mapping" is a direct method in which the Hall probe is assumed to follow the ideal electron trajectory. There is a criterion for the choice of the step size S_{i0} for the integral strength accuracy,but it does not influence the precision of the results when one translate them from "radial" to "lamination" mapping.

The sextupole field behavior (Fig. 4) at the magnet edge is very different [9,10] between the measurements performed with the "Radial" and the "Lamination" Mapping methods. This behavior originates from the coil which produces a pole face bent. When entering the end field region and then moving away from the magnet, the field on the nominal trajectory initially decreases rapidly, then goes to smaller negative values and then tends asymptotically to zero (Fig. 2). Therefore, if the field is mapped along the lamination direction x-axis, the effective magnet pole face is bent symmetrically (Fig. 5a). Therefore, the measured field behavior is also symmetric [2]. Owing to this reason, the sextupole component d^2B/dx^2 along the longitudinal direction as shown in Fig. 4 for the lamination mapping, will have a constant negative sign in the edge region.

However, if the field is mapped along the radial

Table 1
The integrated harmonic field strength obtained from the different measurement and analysis methods

Harmonic field	Eq. (19)			Eq. (22)			Eq. (25)			Eq. (31)		
	$\Theta \leq -10°$	$10° \geq \Theta \geq -10°$	$\Theta \geq 10°$	$\Theta \leq -10°$	$10° \geq \Theta \geq -10°$	$\Theta \geq 10°$	$\Theta \leq -10°$	$10° \geq \Theta \geq -10°$	$\Theta \geq 10°$	$\Theta \leq -10°$	$10° \geq \Theta - 10°$	$\Theta \geq 10°$
$\int Bds$ [T B]	0.0277	1.4648	0.0268	0.0277	1.4648	0.0268	0.0277	1.4647	0.0269	0.0277	1.4647	0.0269
$\int Gds$ [T]	−0.081	−2.255	−0.081	−0.081	−1.836	−0.081	0.009	−1.998	0.009	0.009	−1.999	0.009
$\int Sds$ [T/m]	−0.32	−0.51	−0.29	−0.30	−1.13	−0.30	−0.48	−0.75	−0.46	−0.49	−0.73	−0.47
$\int Ods$ [T/m^2]	3.9	18.4	1.1	1.5	18.0	1.7	1.5	12.7	0.7	1.0	13.5	0.6
$\int Dds$ [T/m^3]	−47	−78	−103	−63	−114	−61	−24	−100	−85	−37	−115	−39

Table 2
The integrated harmonic field strength after the analysis treatments

Harmonic field	Eq. (20)	Eq. (23)	Eq. (30)	Eq. (30)
$\int B ds$ [T B]	1.5193	1.5193	1.5193	1.5193
$\int G ds$ [T]	−1.979 (−2.417)	−1.980 (−1.998)	−1.985 (−1.979)	−1.986 (−1.980)
$\int S ds$ [T/m]	−1.12	−1.16 (−1.73)	−1.69	−1.69
$\int O ds$ [T/m^2]	23.4	21.2	14.9	15.1
$\int D ds$ [T/m^3]	−228	−199	−209	−191
L_{eff} [m]	1.2219	1.2219	1.222	1.222

( ) without modification.

direction r-axis, the effective magnet pole face is bent but not symmetric (Fig. 5b). Hence, the measured field is not symmetric with respect to the radial direction. Therefore, the sextupole component d^2B/dr^2 changes sign in the edge region is shown in Fig. 4 [10,11]. Table 2 indicates that the sextupole strength measured by the radial mapping trajectory with the different analysis method can be adjusted by means of Eq. (23) and the corresponding result for $\int S\, ds$. As revealed in this table, the results between the two analysis methods on the same radial mapping are consistent. The sextupole strength from Eq. (25) and Eq. (31) on the lamination mapping are the same, and slightly larger than the results from Eq. (19) and Eq. (23) on the radial mapping. This slight difference originates from the different mapping trajectories which allow the Hall probe to take the different fringing field behavior at the edge of coil. For higher multipoles beyond the sextupole, the modification factor entering in the analysis of the lamination mapping is so small that it can be neglected.

For beam optics studies, the field expansion along the radial direction given in Table 2 is the one of interest. The sextupole strength is very strong at the magnet edges but rather weak in the center region (Fig. 4). Therefore, the edge effect can be treated separately as a thin lens located on both sides of the dipole magnet [11]. One can also use end shims to compensate this strong negative sextupole field [2]. Notably the edge sextupole fields have a net

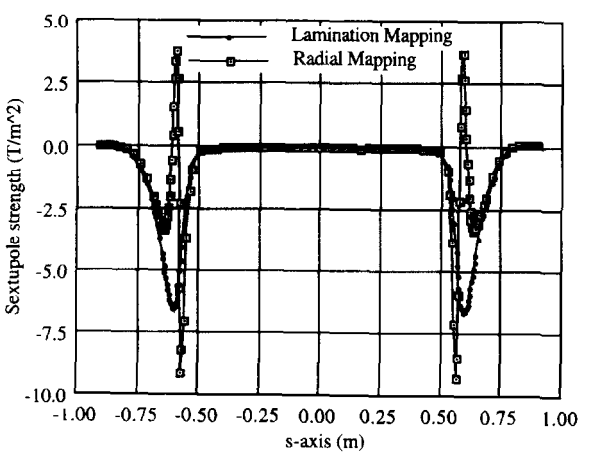

Fig. 4. Sextupole field distribution along the longitudinal direction of the two mapping methods.

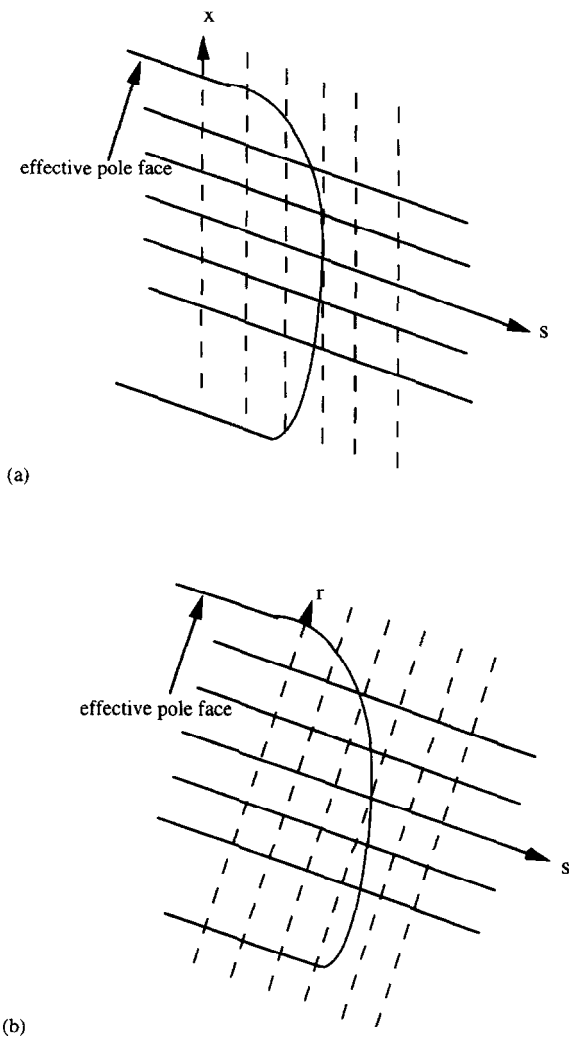

Fig. 5. (a) The relation between the effective magnet pole face and mapping trajectories under the lamination mapping method. (b) The relation between the effective magnet pole face and mapping trajectories under the radial mapping method.

positive effect on the chromaticities [11]. However, if the shims were added at the magnet edges, a wider good field region would be obtained.

5. Conclusions

Since the combined function bending magnet with rectangular hard-edge has a gradient field, a good alignment must be achieved between the magnet and the Hall probe bench to ensure that the mapping will pass through the exact magnet center and follow the nominal trajectory. The measurement results indicate that the dipole field strength does not depend on the different analysis methods. Those results conform not only that the measurement system is of high precision, but also that the analysis methods are reliable. However, the field measurement with the different methods reveals that the multipole strength at the two edges is quite different, particularly for the sextupole field. But using a proper analysis method transforms the measurement results into the final solution, the final analysis results are all consistent between the different methods discussed in Section 3.1 and Section 3.2. However, a small difference exists between the "Radial" and "Lamination" Mapping methods. The multipoles higher than the sextupole is independent of the different mapping method. This is because that end field difference between these two mapping methods of the multipoles higher than the sextupole is less sensitive to the sextupole.

The difference in the gradient field integral between "Radial" and "Lamination" Mapping is about 0.3%. The sextupole end field depends strongly on the mapping method, but it is qualitatively well understood. After a proper analysis treatment of the measurements, the four methods give consistent results. Therefore the difference in the integrated sextupole strengths remains in the order of 0.54 T/m between the two mapping methods. However, since the radial mappings in the most natural are concerning beam dynamic's calculation, the corresponding results are to be used. This is true for the higher multipole content.

However, according to the magnet construction, the lamination mapping is deemed in this study to be of great interest and to more thoroughly understand the entire magnet performance. Moreover, using a proper corresponding analysis method of the data has determined the quality and reliability of the measurement bench.

Acknowledgments

The authors are indebted to Dr. C.S. Hsue and C.C. Kuo as well as Mr. J.C. Lee of the Beam Dynamics Group for useful discussion regarding the analysis of the mapping data of the dipole magnet and also thank Mr. C.T. Fan, F.Y. Lin and Mrs. Sheting Yeh for their technical support.

References

[1] C.H. Chang, H.C. Liu and G.J. Hwang, Proc. 1993 Part. Accel. Conf. 4 (1993) p. 2886.
[2] C.S. Hwang, C.H. Chang, G.J. Hwang, P.K. Tseng and T.M. Uen, 14th Int. Conf. Magnet Technology, Finland, June 11–16, 1995.
[3] C.S. Hwang, W.C. Chou, J.H. Huang, M.Y. Lin, T. Chang and P.K. Tseng, 11th Int. Conf. on Magnet Technology (MT-11), Japan (1989) p. 291.
[4] C.S. Hwang, F.Y. Lin, G.J. Jan and P.K. Tseng, Rev. Sci. Instr. 65 (1994) 2548.
[5] C.S. Hwang, W.C. Chou, J.H. Huang, G.J. Jan and P.K. Tseng, 3rd ROC-ROK Metrology Symp., Taiwan (1990) p. 69.
[6] C.S. Hwang, W.C. Chou, J.H. Huang and P.K. Tseng, SRRC Internal Report, SRRC-MM-IM-90-01 (1990).
[7] M. Conte and W.W. Mackay, An introduction to the Physics of Particle Accelerators (World Scientific, 1991).
[8] P.K. Tseng and C.S. Hwang, XVth Int. Conf. On High Energy Accelerators, Vol. 1 (1992) p. 598.
[9] K. Halbach, Nucl. Instr. and Meth. A 248 (1986) 429.
[10] S. Caspi, M. Helm and L.J. Laslett, SC-MAG-328, LBL-30313 (1991).
[11] J.C. Lin, Proc. Part. Accel. Conf., San Francisco, May 6–9 (1991).